22 May 2006

Molecular Dynamics of Polystyrene Solutions in Microwave Fields

Mark J. Purdue

James M. D. MacElroy

D. F. O'Shea

Macduff O. Okuom

et. al. For a complete list of authors, see https://scholarsmine.mst.edu/chem_facwork/2370

Recommended Citation

M. J. Purdue et al., "Molecular Dynamics of Polystyrene Solutions in Microwave Fields," *Journal of Chemical Physics*, American Institute of Physics (AIP), May 2006.
The definitive version is available at https://doi.org/10.1063/1.2197496

Molecular dynamics of polystyrene solutions in microwave fields

Mark J. Purdue, J. M. D. MacElroy,[a] and D. F. O'Shea
UCD School of Chemical and Bioprocess Engineering, The Centre for Synthesis and Chemical Biology, Conway Institute of Biomolecular and Biomedical Research, University College Dublin, Belfield, Dublin 4, Ireland

Macduff O. Okuom and Frank D. Blum
Department of Chemistry, University of Missouri-Rolla, Rolla, Missouri 65401-0010 and Graduate Center for Materials Research, University of Missouri-Rolla, Rolla, Missouri 65401-0010

(Received 26 January 2006; accepted 28 March 2006; published online 22 May 2006)

Equilibrium and nonequilibrium molecular dynamics simulation techniques were used to assess the influence of an applied microwave field on the dynamics of methylamine-methanol and methylamine-dimethylformamide (DMF) solutions bound within atactic polystyrene over a range of polymer densities from 35 to 96 wt % polymer. Atomistically detailed systems were studied, ranging from 3000 to 10 644 particles, using previously established potential models. Structural and dynamical properties were determined in the canonical (*NVT*) ensemble at 298 K. The simulated DMF self-diffusion coefficients in polystyrene solutions were compared with the zero-field experimental results established with pulsed-gradient spin-echo NMR spectrometry. A simulated external microwave field, with a rms electric field intensity of 0.1 V/Å, was applied to these systems and the simulated dynamical results over field frequencies up to 10^4 GHz were compared with the zero-field values. Simulated evidence of athermal effects on the diffusive characteristics of these mixtures is reported. © *2006 American Institute of Physics*. [DOI: 10.1063/1.2197496]

INTRODUCTION

Applications in science and engineering which rely on an understanding of the fundamental phenomena controlling diffusive transport in polymeric media are widespread and include such diverse fields as drug delivery,[1–3] optoelectronic devices,[4,5] and organic synthesis.[6–10] It is therefore not surprising that diffusion of low molecular weight solutes and solvents within polymers has been very widely studied for many decades. To date much of this work has involved transport in the absence of external fields, however, recent studies have suggested that significantly enhanced transport and/or reaction rates may be achieved in such systems in the presence of applied microwave or far infrared electromagnetic fields. For example, in Ref. 11 microwaves were employed to control the permeation of CO_2 gas in a cellulose acetate membrane. In this experimental study, polar hydroxyl groups bound within the polymeric membrane were active in the microwave field. Upon irradiation of the membrane, the polymer temperature and free volume were found to increase, the degree of which depended on the microwave power. A polystyrene membrane was chosen as a reference membrane and assumed to be inert to the microwave field and it was found that both diffusion and permeation of CO_2 through the cellulose acetate membrane increased with the field strength, with the enhancement in diffusion being the more remarkable. In another area of growing interest, namely, solid phase organic synthesis (SPOS),[6–10] microwave irradiation has been broadly recognized as a crucial aid to enhancing reaction rates and yields. It is currently believed that this enhancement relies primarily on the ability of the solid/liquid medium to transform the supplied electromagnetic energy into heat. The heat subsequently drives an ongoing chemical reaction between a key reagent and functional groups bound on the polymeric resin, to form druglike molecules which must then be cleaved from the resin after the removal of solvent and excess reagent from the polymer solution. Diffusion of solvents and reagents through the polymeric resin plays a critical role in the success or failure of SPOS.

An open question still exists, however, as to the extent to which nonthermal microwave effects influence the rate processes in these systems at the molecular level and it is this topic which is of primary concern in this paper. In particular, the focus will be on diffusive transport processes as they relate to solid phase organic synthesis since in many cases it is accepted that the organic synthesis rates within these systems are diffusion limited. In order to understand, control, and enhance SPOS with microwave technology, a key issue is the identification of field frequencies and intensities that can accelerate reagent diffusive transport. With this objective in mind, molecular dynamics simulation techniques are employed in this work to investigate the properties of a low concentration methylamine reagent in methanol/polystyrene and dimethyl formamide (DMF)/polystyrene solutions under the influence of an applied microwave field with a rms electric field intensity of 0.1 V/Å and with frequencies ranging up to 10^4 GHz. Solvent/polystyrene solutions were initially solvated under a criterion of balanced chemical potential

[a]Author to whom correspondence should be addressed. Fax: 353-1-7161177; Electronic mail: don.macelroy@ucd.ie

TABLE I. Intramolecular potential parameters for simulations of SPOS mixtures.

Component	Atoms	Parameters (kcal/mol)	Equilibrium angle (°)
Methanol	CH_3-O-H	$k_\theta=55$	$\theta_0=108.53$
DMF	$H-C_o-O$	$k_\theta=50$	$\theta_0=122.5$
	$O-C_o-N$	$k_\theta=80$	$\theta_0=123.0$
	$CH_3^{(2)}-N-C_o$	$k_\theta=70$	$\theta_0=119.0$
	$CH_3^{(1)}-N-C_o$	$k_\theta=70$	$\theta_0=120.0$
	$N-C_o-H$	$k_\theta=50$	$\theta_0=114.5$
	$CH_3^{(1)}-N-CH_3^{(2)}$	$k_\theta=50$	$\theta_0=121.0$
	$O-C-N-CH_3^{(1)}$	$k_\Phi=45/4,\ n_{JK}=2$	$\Phi_0=180$
	$O-C-N-CH_3^{(2)}$	$k_\Phi=45/4,\ n_{JK}=2$	$\Phi_0=180$
	$H-C-N-CH_3^{(1)}$	$k_\Phi=45/4,\ n_{JK}=2$	$\Phi_0=180$
	$H-C-N-CH_3^{(2)}$	$k_\Phi=45/4,\ n_{JK}=2$	$\Phi_0=180$
	C_o, N	$k_\Psi=40$	—
Methylamine	CH_3-N-H	$k_\theta=50$	$\theta_0=121.6$
	H–N–H	$k_\theta=35$	$\theta_0=104.4$
Atactic polystyrene	$CH_2-CH-CH_2$	$k_\theta=60$	$\theta_0=109.5$
	$CH-CH_2-CH$	$k_\theta=63$	$\theta_0=109.5$
	CH_2(al)–CH(al)–C(ar)	$k_\theta=60$	$\theta_0=109.5$
	CH(al)–C(ar)–CH(ar)	$k_\theta=70$	$\theta_0=120.0$
al=aliphatic	$X-CH(al)-CH_2(al)-X$	$k_\Phi=2.8$	$\Phi_0=180$
ar=aromatic	$X-CH(al)-C(ar)-CH(ar)$	$k_\Phi=4$	$\Phi_0=90$
	CH(al)–C(ar)	$k_\gamma=2$	$\chi_0=90.0$
	CH(al)	$k_\omega=50$	—

with the bulk liquid solvent in a field free environment, to accurately predict solvent mobility over a range of polymer densities.

SIMULATION METHODS

Molecular models of solvent and reagent

The three-site united atom optimized potential for liquid simulations (OPLS) model of Jorgensen[12] (designated model J2), the six-site model of Chalaris and Somios,[13] and the four-site united atom model of Impey *et al.*[14] were employed for solvent methanol, solvent DMF, and reagent methylamine, respectively. These potential models employed a 12-6 Lennard-Jones potential function and a Coulombic interaction governed by sets of fixed partial charges located at the center of the atomic nuclei. A harmonic bond angle bending potential function was superimposed on these models to enhance the physical realism without compromising the diffusive characteristics. The spring constants and equilibrium bond angles were taken from the AMBER force field and are detailed in Table I. In addition, DMF contained four-body torsion and inversion potentials, taken from the DREIDING force field,[15] to characterize the planar amide bond. The inversion potential was used in the special form for planar equilibrium. The nitrogen planar bond geometry has been confirmed with x-ray diffraction experiments,[16] although an approximate 15° nonplanarity has been observed with electron diffraction measurements.[17] A third solvent, dichloromethane, shall be considered in future simulation studies.

Molecular model of atactic polystyrene

The molecular dynamics (MD) force field of Mondello *et al.*[18] for atactic polystyrene (*a*-PS) was chosen for the purposes of the present research. This united atom potential model contained no atomic charge sites and therefore ensured that the polymer remained inert to an externally applied e/m field. The atomic centers in real polystyrene have low partial charges and the polymer acts as a poor conductor. As previously mentioned, polystyrene was used as a reference material in the experimental study of the permeation of CO_2 through porous media under an external e/m field.[11] There was no CO_2 mobility enhancement in polystyrene when the e/m field was applied, indicating that the polymer did not indirectly affect the solute dynamics. Based on this experimental evidence, the effect of the external e/m field on polymer solution mobility can be directly associated with solvent/reagent dynamics. The relaxation times for conformational changes in polystyrene chains are on the order of a few nanoseconds, a time scale which is outside the simulation times that have been considered in the current study. Since the relaxation times associated with solvent/reagent molecular motion are considerably smaller, any indirect effect of polymer conformational changes on solute dynamics can be negated within a single 400 ps simulation. Sampling over independent polymer solutions, under an external e/m field, accounts for different molecular phenomena that may be experimentally observable. Therefore, there is no loss of generality when using a charge-free polymer potential model in the current simulations.

A 12-6 Lennard-Jones potential model was used for nonbonded interactions. Harmonic bond angle bending, aliphatic

chain torsions, phenyl ring torsions around CH (aliphatic)-C (aromatic), and improper torsions to maintain the stereochemical configuration of the aliphatic CH groups were all employed to mimic the internal motions in *a*-PS. The Ciccotti algorithm[19] ensured phenyl ring planarity, eliminating the need for a phenyl ring (out of plane) bending potential. POLYPACK was used to generate fully atomistic models of atactic polystyrene.[20] As with previous simulation work on these systems, using the POLYPACK software for polymer structure generation, chains of *a*-PS, each with 40 monomeric units, were constructed with the same rotational isomeric state (RIS) model target values,[21] including an allowance for a shift in configurational statistics upon introducing the MD force field.[22] To characterize the structure of *a*-PS, the carbon-carbon x-ray structure factor was computed at 298 K and was found to be consistent with the results of Mondello *et al.*[18]

Multiple configurations with nine chains of 40 monomeric units were generated using this noncommercial software package over a range of densities with simulation cell sizes up to 50 Å in length. The POLYPACK software, which operated on a UNIX platform, allowed homogeneous structures of specific densities to be rapidly prepared. Larger cell dimensions were prepared by scaling the position of the center of mass of each chain appropriately, while preserving the intrachain relative atomic distances. Taking the carbon centers as the positions of the united atom groups, the relative hydrogen positions along the polymer backbones were recorded. Using the aforementioned united atom MD polystyrene force field, all polymer structures were annealed from a temperature of 500 K down to 300 K using a stepwise cooling regime over the course of 100 ps. Each dry polymer sample was then ready to be solvated and equilibrated in the canonical *NVT* ensemble. The polymer accessible volume Φ_{access} was computed using a Monte Carlo insertion technique, employing 1×10^6 trial insertions and a strict hard-sphere overlap criterion. The volume fraction occupied by the polymer Φ was then determined as $1-\Phi_{\text{access}}$.

Potential energy function

The total potential energy U^{tot} in a polystyrene solution under an applied electromagnetic energy is given by

$$U^{\text{tot}} = U_{\text{LJ}}^{\text{tot}} + U^{\text{Coul}} + U_\theta + U_\phi + U_\psi + U_\omega + U_E, \tag{1}$$

where $U_{\text{LJ}}^{\text{tot}}$ is the shifted force 12-6 Lennard-Jones potential, U^{Coul} is the pairwise additive Coulombic potential, U_θ, U_ϕ, U_ψ, and U_ω are bond angle bending, torsion, inversion, and improper torsion potentials, respectively, and U_E is the electric potential due to the external field. The potential energy term due to the magnetic component of the e/m field is dependent on the orientation of a magnetic dipole moment relative to the alternating magnetic field. In turn, the magnetic dipole moment is related to the current and area of a current loop which is a complex entity not readily accessible in classical simulations. However, the effect of the electric field on molecular properties of polar fluids is orders of magnitude greater than that of the magnetic field.[23] The magnetic potential energy is therefore excluded in Eq. (1) without loss of generality to the simulated effects of e/m fields,

$$U_{\text{LJ}}^{\text{tot}} = \sum_{i=1}^{N}\sum_{j<i} U_{\text{LJ},ij}^{\text{SF}} + \sum_{a=1}^{n\ \text{type}(a)}\sum_{b<a} U_{\text{LJ},ab}^{\text{LRC}}, \tag{2}$$

where

$$U_{\text{LJ},ij}^{\text{SF}}(r_{ij}\leqslant R_{\text{cut}}) = 4\varepsilon_{ij}\left[\left(\frac{\sigma_{ij}}{r_{ij}}\right)^{12} - \left(\frac{\sigma_{ij}}{r_{ij}}\right)^{6}\right] - U_{\text{LJ},ij}|_{r_{ij}=R_{\text{cut}}} - (r_{ij}-R_{\text{cut}})\left|\left(\frac{dU_{\text{LJ},ij}(r_{ij})}{dr_{ij}}\right)\right|_{r_{ij}=R_{\text{cut}}}, \tag{3}$$

$$U_{\text{LJ},ij}^{\text{SF}}(r_{ij} > R_{\text{cut}}) = 0, \tag{4}$$

and the Lorentz-Berthelot mixing rules apply

$$\varepsilon_{ij} = \sqrt{\varepsilon_i \varepsilon_j}, \tag{5}$$

$$\sigma_{ij} = \left(\frac{\sigma_i + \sigma_j}{2}\right), \tag{6}$$

and the long-range correction is

$$U_{\text{LJ},ab}^{\text{LRC}} = \left(\frac{8\pi N_a N_b}{9V}\right)\left[\left(\frac{\sigma_{ab}}{R_{\text{cut}}}\right)^9 - 3\left(\frac{\sigma_{ab}}{R_{\text{cut}}}\right)^3\right]\sigma_{ab}^3\varepsilon_{ab}, \tag{7}$$

where N_a is the number of molecules of type a and V is the volume of the simulation cell,

$$U^{\text{Coul}} = \sum_{i=1}^{N}\sum_{j<i}\frac{q_i q_j}{4\pi\varepsilon_0 r_{ij}}, \tag{8}$$

where q_i denotes an atomic charge site and ε_0 denotes the permittivity of free space. The simple Coulombic potential described the electrostatic interactions associated with whole solvent and reagent molecules only. The nearest image convention was employed for the electrostatic interactions of the penetrant species in polymer solutions.[24] The bond angle bending potential was represented as follows:

$$U_\theta = \tfrac{1}{2}\sum_{i=1}^{n\ \text{angles}} k_{\theta,i}[\theta_i - \theta_{i,0}]^2, \tag{9}$$

where θ_i and $\theta_{i,0}$ represent the actual and equilibrium *external* angles of angle number i and $k_{\theta,i}$ denotes the corresponding spring constant. The torsion potential was represented as follows:

$$U_\phi = \tfrac{1}{2}\sum_{i=1}^{n\ \text{torsions}} k_{\phi,iJK}[1 - f_{iJK}(\phi_i)] \tag{10}$$

and

$$f_{iJK}(\phi_i) = \begin{cases} \cos[n_{iJK}(\phi_i - \phi^0_{iJK})], & JK \in \text{liquid} \\ \cos(3\phi_i), & J{:}K \Leftrightarrow \text{CH}_2\text{(aliphatic):CH(aliphatic)} \\ \cos^2(\phi_i), & J{:}K \Leftrightarrow \text{CH(aliphatic):C(aromatic)}, \end{cases} \tag{11}$$

where ϕ^0_{iJK} denotes an equilibrium dihedral angle with central atoms J and K; n_{iJK} and $k_{\phi,iJK}$ denote the periodicity and partial rotation barrier of the same torsion type. The partial rotation barrier is simply the total rotation barrier divided by the number of possible torsions in the molecule with I and L atoms. The DREIDING torsional parameters, which were used for liquid DMF, were obtained from hybridization theory.[15] The inversion potential for an atom I, bonded to exactly three other atoms, J, K, and L, was used in the special form for planar equilibrium and is given as follows:

$$U_\psi = \sum_{i=1}^{n \text{ inversions}} k_{\psi,i}[1 - \cos \psi_i], \tag{12}$$

where ψ_i denotes the angle between the IL bond and the JIK plane, and $k_{\psi,i}$ denotes the corresponding inversion barrier. To maintain the stereochemical configuration about the phenyl-ring connecting carbon atom, an improper torsion potential was also introduced. This required *a priori* knowledge of typical relative hydrogen atom positions, which was obtained from the original POLYPACK configurations and maintained constant throughout the MD simulations. The improper torsion potential is expressed as follows:

$$U_\omega = k_\omega \sum_{i=1}^{n \text{ improper}} \omega_i^2, \tag{13}$$

where ω_i denotes the improper torsion angle which measures the angle between the normal to the plane formed by three successive backbone carbon atoms and the equilibrium direction of this normal (corresponding to 35.04° to the direction of the hydrogen atom bonded to the central carbon atom, which would have been present if it had been explicitly simulated). The electric potential is defined as

$$U_E(t) = -\mathbf{M} \cdot \mathbf{E}(t) = -M_z E(t), \tag{14}$$

where $\mathbf{M} = M_x\mathbf{i} + M_y\mathbf{j} + M_z\mathbf{k}$ is the total dipole moment vector of the entire system, arising from the sum of the individual permanent molecular dipole moment vectors $\boldsymbol{\mu}_i$,

$$\mathbf{M} = \sum_{i=1}^{N_{\text{mol}}} \boldsymbol{\mu}_i, \tag{15}$$

and the electric dipole moment of molecule i consisting of n_{atom} atoms is given by

$$\boldsymbol{\mu}_i = \sum_{i=1}^{n_{\text{atom}}} \mathbf{r}_i q_i. \tag{16}$$

Using the potential function given by Eq. (1), and the potential parameters cited in Table I, MD simulations of polymer solutions in an external e/m field were performed.

Upon examination of Lennard-Jones potential energy curves for both the liquids and polymer, the cut-off radius for LJ interactions within either the liquid or polymer components was set at $R_{\text{cut}} = 10.5$ Å for methanol solutions and 15.0 Å for DMF solutions. The Lorentz-Berthelot mixing rules[24] were applied for interactions between different types of Lennard-Jones (LJ) sites within the same or across different components. All subsequent MD simulations were performed in the canonical *NVT* ensemble using a Nosé-Hoover chain of five thermostats with a fluctuation period of 0.5 ps. Excellent temperature control was achieved in the simulations with a rms temperature fluctuation of no more than 7 K in any of the simulations presented herein. After comparisons between results with and without long-range electrostatic interactions, it was decided to use the simple Coulombic potential for the calculations of excess chemical potential and for the non-equilibrium molecular dynamics (NEMD) simulations. The comparison was made for the molecular MSD at the highest simulated polymer density and the result obtained with the Lekner summation method[25] was approximately 20% larger. This deviation is expected to reduce considerably as the polymer box size increases and consequently the size of the truncation error associated with the nearest image convention reduces. Under zero field conditions, each dry polymer configuration was solvated and the resulting polymer solutions were equilibrated for 120 ps, where the latter 100 ps were also used in the calculations of the solvent excess chemical potential. A single methylamine reagent was then randomly inserted into each polymer solution before a further equilibration period of 10 ps in the appropriate e/m field environment. This sequence was followed by a production period of 400 ps during which the dynamical and structural features of these SPOS mixtures were investigated. A single time step scheme was used with steps of 1.0 fs over the course of all the simulations. Additional methods are outlined next to obtain useful structural and dynamical information.

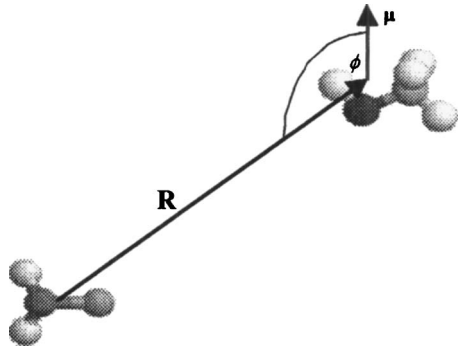

FIG. 1. Orientation of a single methanol molecule about a single methylamine molecule.

TABLE II. Methanol and DMF atomic force field parameters at $\lambda=1$. $e\approx1.6022\times10^{-19}$ C; Me=united methyl group.

Methanol atoms	ε/k_B (K)	σ (Å)	q (e)	DMF atoms	ε/k_B (K)	σ (Å)	q (e)
O	85.61	3.2400	−0.700	O	100.00	2.9600	−0.500
Me	104.24	3.8600	0.265	C	50.00	3.7000	0.450
H	0.00	0.0000	0.435	H	8.00	2.2000	0.060
				N	80.00	3.2000	−0.570
				Me	80.00	3.8000	0.280

Orientational motion

The normalized average molecular electric dipole moment autocorrelation function (ACF) is determined as

$$\phi(t)=\frac{\langle\boldsymbol{\mu}_l(t)\,.\,\boldsymbol{\mu}_i(0)\rangle}{\langle\boldsymbol{\mu}_l(0)\,.\,\boldsymbol{\mu}_i(0)\rangle}. \tag{17}$$

Orientational relaxation times in methanol and DMF were determined using the following relations:

$$\tau_l=\int_0^\infty C_l(t)dt, \tag{18}$$

where

$$C_l(t)=\langle P_t(\cos[\theta(t)])\rangle, \tag{19}$$

where $\theta(t)$ is the angle through which a molecule-fixed vector $\mathbf{e}_i$ rotates in a time t: $\cos[\theta(t)]=\mathbf{e}_i(t)\cdot\mathbf{e}_i(0)/|\mathbf{e}_i(t)||\mathbf{e}_i(0)|$ and $P_1(x)=x; P_2(x)=(3x^2-1)/2$. The rotational diffusion coefficient D_R can be estimated for the particular orientational motion under study using the following relation:

$$D_R=\frac{1}{l(l+1)\tau_t}. \tag{20}$$

Equation (20) was used to determine the influence of the e/m field on the rotational behavior of methanol and DMF in a range of polystyrene solutions at different polymer densities, despite the penetrant molecular species having flexible bond angles. However, this oversight was not deemed to be significant due to the high frequency of motion associated with bond angle bending and rotational motion of penetrant molecules could still be examined.

Solvent cosphere of the reagent

The radius of the solvent cosphere of the reagent was taken as the average distance between the center of mass (c.m.) of the reagent to the crossover of the solvent c.m. first solvation shell with the ideal gas value of unity, as determined from analysis of radial distribution functions (RDF) analysis. The orientation of solvent molecules about the reagent within the first solvation shell of the reagent can be characterized with the geometric illustration shown in Fig. 1.

One can examine the dot product: $\cos(\phi)=\boldsymbol{\mu}.\mathbf{R}/|\boldsymbol{\mu}||\mathbf{R}|$. The vector $\mathbf{R}$ denotes the vector from the c.m. of the reagent to the c.m. of a solvent molecule within the solvent cosphere of the reagent. The vector $\boldsymbol{\mu}$ denotes the molecular electric dipole moment vector. The angle between $\mathbf{R}$ and $\boldsymbol{\mu}$ indicates how solvent dipoles geometrically organize themselves about the reagent. Of further interest was the average residence time of a solvent molecule within the defined cosphere of the reagent. A residence time distribution (RTD), with probability $P(t)$, was determined and a mean residence time computed using the following relationship:

$$\langle\tau_{\mathrm{RT}}\rangle=\frac{\int_0^\infty P(t)tdt}{\int_0^\infty P(t)}. \tag{21}$$

TABLE III. λ scaling of nonbonded parameters: $0\leqslant\lambda\leqslant1$. The subscript "org" denotes an original full potential parameter defined in Table II. $F_\lambda=[f_{\mathrm{RD}}+(1-f_{\mathrm{RD}})\lambda]$. Values of $f_{\mathrm{RD}}=0.8$ for methanol and $f_{\mathrm{RD}}=0.9$ for DMF were used.

Parameter	Hydrogen, H	Nonhydrogen, I	Polymer, P
ε	$\lambda^2\varepsilon_{\mathrm{H,org}}$	$\varepsilon_{I,\mathrm{org}}$	$\varepsilon_{P,\mathrm{org}}$
σ	$\sigma_{\mathrm{H,org}}$	$F_\lambda\sigma_{I,\mathrm{org}}$	$\sigma_{P,\mathrm{org}}$
q	$\lambda q_{\mathrm{H,org}}$	$\lambda q_{I,\mathrm{org}}$	⋯

Polymer structure

In an effort to characterize the structure of a-PS, the carbon-carbon radial distribution function shall be determined. This accounts for both backbone and side chain carbon atoms. For direct comparison with experiment, the carbon-carbon x-ray structure factor was also computed using the following form:

$$S_{ij}(q)=\delta_{ij}+\langle\rho_j\rangle\int 4\pi r^2[g_{ij}(r)-1]\frac{\sin(qr)}{qr}dr, \tag{22}$$

where q is the scattering vector ($=4\pi\sin\theta/\lambda$), $\langle\rho_j\rangle$ is the average density of atom j, $g_{ij}(r)$ is the radial distribution function, and δ_{ij} is the Kronecker delta.

Excess chemical potential

In order to balance the solvent chemical potential between the bulk solvent and each polymer solution at thermal and mechanical equilibria, it is necessary to compute the solvent excess chemical potential. Due to computational demands on achieving this balance with each polymer solution, an assumption was made that the chemical potential was identical with and without the field environments studied in this research. A two-step method suitable for high density systems[26] that combines the Widom particle insertion technique with the method of thermodynamic integration, was used in this research to compute the solvent excess chemical potential.

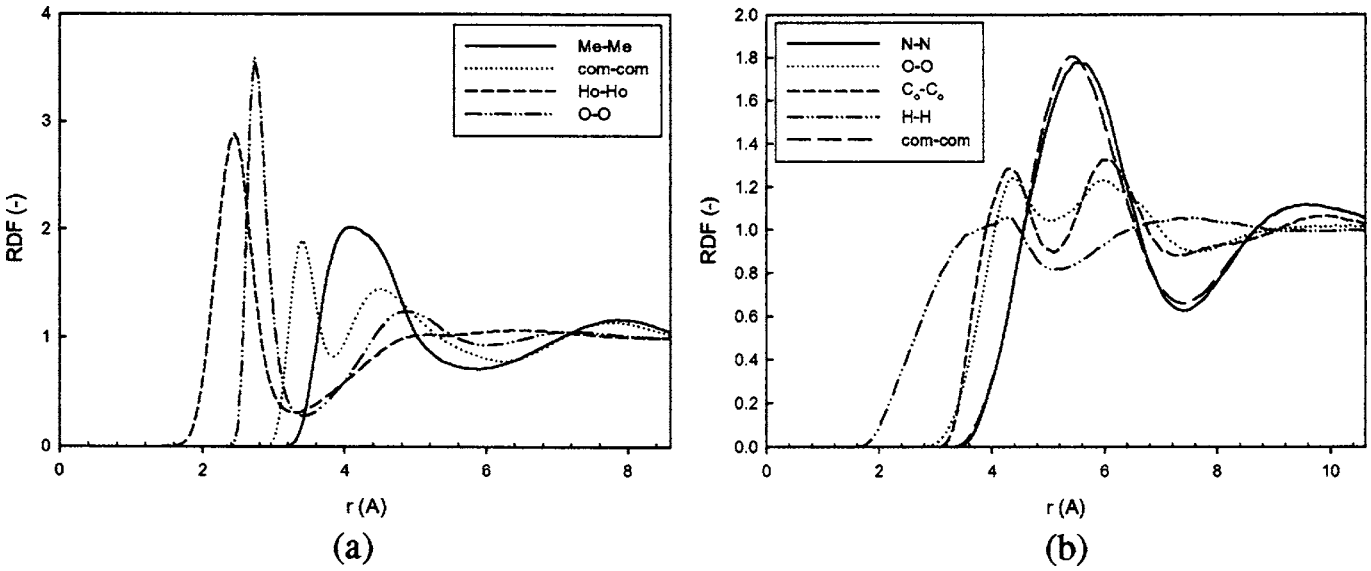

FIG. 2. Homoatomic radial distribution functions in bulk solvents at 25 °C obtained from MD simulations: (a) methanol at 0.79 kg/m^3 and (b) DMF at 0.94 kg/m^3.

The method involves a scaling parameter λ to slowly reduce the solvent particle radii towards a noble state. The internal degrees of freedom of any molecule were independent of this scaling parameter. Analytical expressions for the derivative of the λ-dependent potential energy with respect to λ, were derived for the molecular model.[27] Five steps along a thermodynamic path, equidistant in λ, were employed between unity and zero. The numerical values of the full interaction parameters are shown in Table II and the scaling relations for the three types of atoms relevant to this method are shown in Table III: H denotes any hydrogen atom in the liquid component, *I* denotes a nonhydrogen atom in the liquid component, and *P* denotes any atom in the polymer component. Finally, based upon equality of chemical potential, the equilibrium loadings for each solvent in the various polymer chain configurations were determined.

External electromagnetic field

A plane polarized alternating electromagnetic (e/m) field was applied uniaxially in the z direction, with the plane of polarization in the xz plane. Since the charge sites were coincident with the nuclear degrees of freedom, the electromagnetic force acting upon a site i was superimposed upon forces arising under field absent conditions,

$$m_i\ddot{\mathbf{r}}_i = \mathbf{f}_i + q_i\mathbf{E}(t) + q_i\mathbf{v}_i \times \mathbf{B}(t), \tag{23}$$

where the electric and magnetic field intensities are defined as

$$\mathbf{E}(t) = E_{\max}\cos(\omega t)(0\mathbf{i} + 0\mathbf{j} + 1\mathbf{k}),$$

$$\mathbf{B}(t) = B_{\max}\cos(\omega t)(0\mathbf{i} + 1\mathbf{j} + 0\mathbf{k}), \tag{24}$$

with the maximum electric and magnetic field intensities, $E_{\max}$ and $B_{\max}$, and the angular frequency ω obtained as

$$E_{\max} = \sqrt{2}E_{\mathrm{rms}}, \quad B_{\max} = E_{\max}/c, \quad \omega = 2\pi\nu, \tag{25}$$

where E_{rms} is the root mean square electric field intensity (V/Å), c is the speed of light (m/s), and ν is the frequency (GHz). The incorporation of the e/m field into the MD simulations was accomplished in an explicit manner that has been detailed in previous research on MD simulations of the microwave heating of water.[23]

Diffusion in polymers

In the laboratory frame of reference, at constant temperature, the molar diffusion flux of component i is given by

$$\mathbf{J}_i = -\sum_{j=1}^{\kappa} L_{ij}\nabla_T\mu_j, \tag{26}$$

where μ_j is the chemical potential of component j and the phenomenological coefficients are given by the Einstein form

$$L_{ij} = \frac{1}{6Vk_BT}\lim_{t\to\infty}\frac{d}{dt} \times \left\langle \sum_{k=1}^{N_i}[\mathbf{r}_{ki}(t) - \mathbf{r}_{ki}(0)] \cdot \sum_{l=1}^{N_j}[\mathbf{r}_{ij}(t) - \mathbf{r}_{ij}(0)] \right\rangle. \tag{27}$$

Equation (27) contains cross and self terms which contribute to the flux of a component within the four component system (trace solvent/collective solvent/reagent/polymer). Under conditions of conservation of total linear momentum and in-

TABLE IV. Molecular and total fluid electric dipole moments.

Component	μ^{liq} (D)	μ^{gas} (D)	$\lvert\mathbf{M}\rvert$ (D)
Methanol	2.25	1.70	54.3
DMF	4.33	3.79	82.4
Methylamine	1.30	1.31	20.5

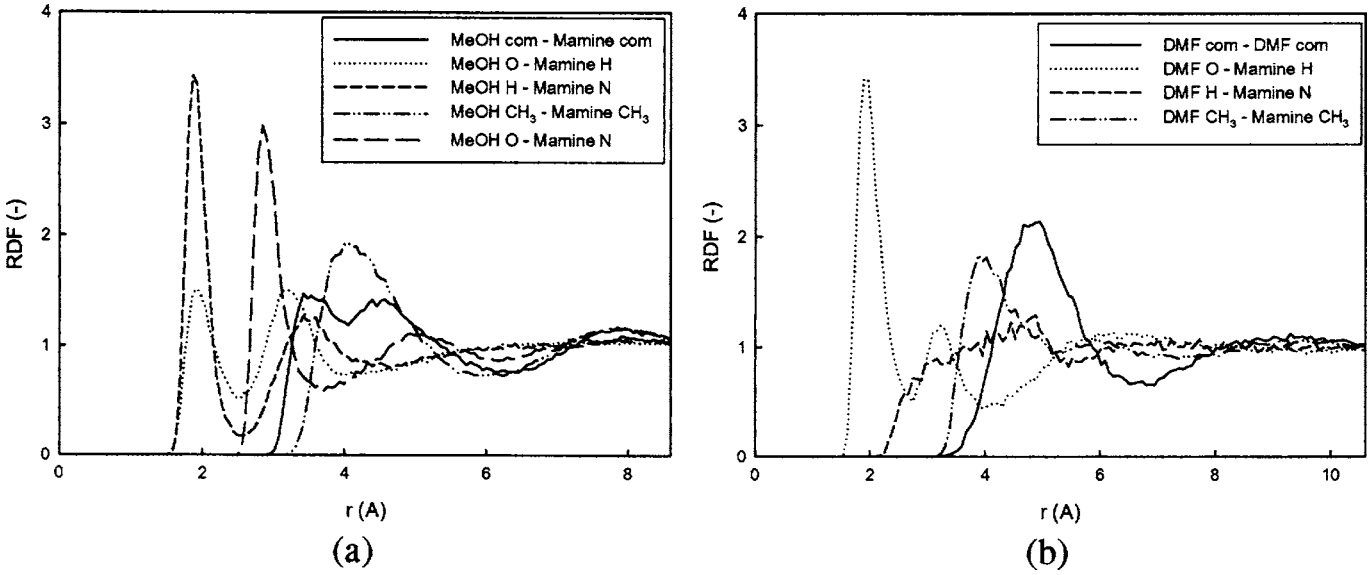

FIG. 3. RDFs in binary liquid mixtures at 25 °C: (a) methylamine-methanol and (b) methylamine-DMF.

corporating the Gibbs-Duhem relation, these terms and the potential gradients in Eq. (26) are related. In this study, the results of solvent and reagent self-diffusion shall be presented, having established negligible collective polymer motion. Equation (27) demonstrates the need for significantly long simulation times to correctly determine the limiting slope of the ensemble averaged cross-time-displacement in the Fickian regime of diffusion. In free flight, the distance traveled by a particle is linear in time and the mean squared displacement is quadratic. Between this ballistic regime and the long-time Fickian regime, where the mean squared displacement is linear in time, there is anomalous diffusion and the mean squared displacement obeys a power law in time with an exponent less than unity. This regime becomes apparent when some feature of the environment interrupts a particle's random walk and is the case for a penetrant confined within a polymer cavity. The diffusion coefficient can still be estimated provided a general model can be assumed which incorporates the long-time behavior of the penetrant. An overview analysis of several simulation results from the literature (both from MD and multidimensional transition-state theory) was conducted in this research. It was determined that the best model to use when approaching Fickian diffusion from the anomalous regime is a simple linear combination of both diffusive regimes

$$\langle \Delta \mathbf{r}^2(i) \rangle = \frac{1}{N} \sum_l |\mathbf{r}_l(t) - \mathbf{r}_i(0)|^2 = At + Bt^n, \tag{28}$$

where n was determined to be 0.5, consistent with a value for purely anomalous diffusion. This value of n was determined using a nonlinear least squares analysis of scanned MSD results for various polymer/solvent systems covering the penetrants: helium, hydrogen, oxygen, argon, water, methane, and ethanol in the polymers: polyamide,[28] polycarbonate,[29,30] poly(dimethylsiloxane),[31,32]

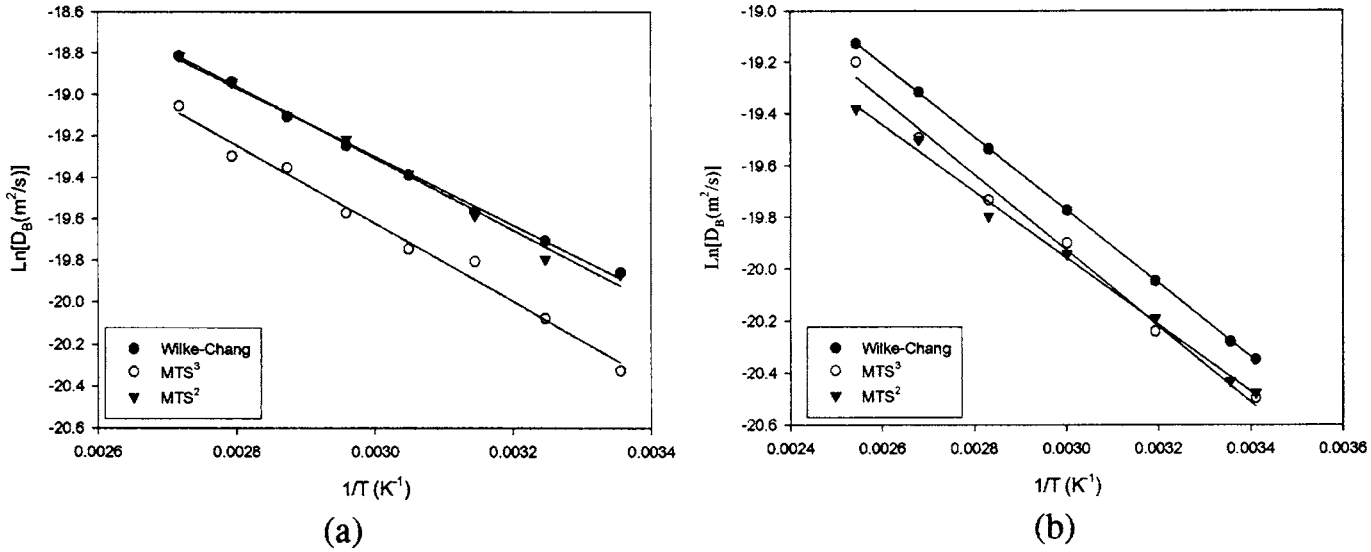

FIG. 4. Arrhenius plot of self-diffusion coefficient in bulk solvents: (a) methanol and (b) DMF.

TABLE V. Solvent Arrhenius parameters: preexponential factors D_0 (m^2/s) and activation energies E_D (J).

	Method	Methanol	DMF
$D_0/10^{-7}$ (m^2/s)	Wilke-Chang	5.87	1.79
	MTS[3]	8.29	1.79
	MTS[2]	7.40	0.98
$E_D/10^{-20}$ (J)	Wilke-Chang	2.28	1.95
	MTS[3]	2.59	2.02
	MTS[2]	2.39	1.76

polyisobutylene,[33] and polypropylene.[34–36] All of these polymers held significantly large pendant side groups decorated along the polymer backbones, comparable with the bulky phenyl groups in polystyrene. In addition to the data produced in this research, the referenced literature data were correlated with Eq. (28). The Levenburg-Marquardt algorithm[37] was used to obtain convergence on the values of the three parameters $\{A,B,n\}$, where the parameter $A(Å^2/ps)=(3/5)D(10^{-9}\ m^2/s)$ and the regression analysis incorporated the Jacobian matrix corresponding to the generic model given by Eq. (28).

Diffusion in polymers has also been examined using phenomenological descriptions, which lack detailed molecular information about the polymer. The free volume theory[38] has perhaps become the most prominent of such methods whereby the solvent self-diffusion coefficient in a solvent(1)/polymer(2) system is given by the following linear form:

$$\frac{(1-\omega_1)}{\ln(D_1/D_B)} = A'\omega_1 + B' \ \text{(constant } T\text{)}, \tag{29}$$

where the solvent self-diffusion coefficient D_1 has been normalized by the solvent self-diffusion coefficient in the bulk liquid phase D_B. An even simpler model based on polymer free volume is the simple geometric relation given by the parameter-free Mackie-Mears lattice model,

$$\frac{D_1}{D_B} = \left(\frac{1-\Phi}{1+\Phi}\right)^2, \tag{30}$$

where Φ is the polymer volume fraction. The diffusivity of benzene in *a*-PS relative to the bulk solvent self-diffusivity at 300 K and polar solvent/polyvinylacetate (PVA) were both well represented by the Mackie-Mears lattice model.[39] Equations (29) and (30) can be examined further in the current research to determine how these models compare to systems constituting a polar solvent (methanol/DMF) solvated in a nonpolar polymer (polystyrene).

RESULTS

Validation of pure species potential models

In preparation for MD simulations of ternary component mixtures, the results of pure species and binary mixture MD simulations at 25 °C are discussed next. Bulk liquid simulations contained 256 molecules.

Liquid structure

For liquid methanol in Fig. 2(a), the hydroxyl hydrogen (H_o) homoatomic RDF peaks at about 2.2 Å, in contrast to a peak in the methyl group at 4.2 Å. The size of hydroxyl hydrogens relative to bulky methyl (Me) groups allows a much closer proximity to each other with the former. For liquid DMF in Fig. 2(b), the computed RDFs are very similar to the results of Chalaris and Samios.[13] As expected, the homoatomic nitrogen RDF closely follows the c.m. RDF and the homoatomic oxygen RDF also closely follows the homoatomic carbonyl carbon RDF, but with less structure due to its peripheral location on the DMF molecule. In addition for liquid DMF, the homoatomic hydrogen RDF contains two solvation layers with significantly less structure than with either oxygen or carbonyl carbon (C_o). This reduction in structure can be attributed to the peripheral location of hydrogen, lack of hydrogen-bonding, and its small atomic radius.

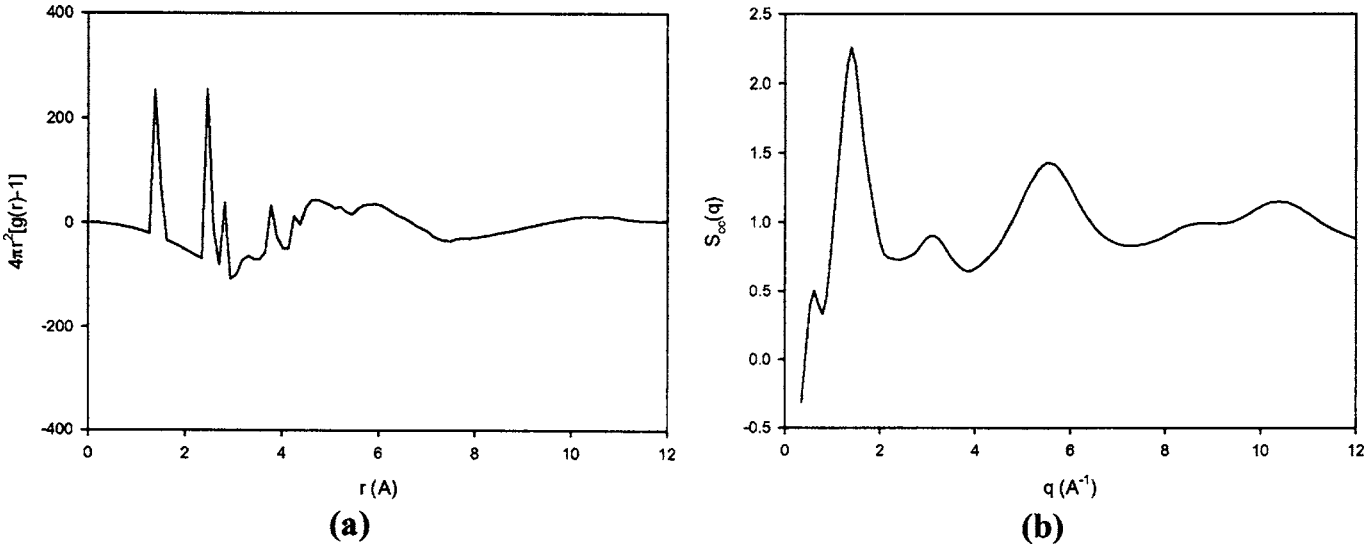

FIG. 5. Carbon-carbon structure in bulk *a*-PS at 25 °C and 0.97 kg/m^3 obtained from MD simulations: (a) RDF and (b) x-ray structure factor.

TABLE VI. Methanol and DMF.

L (Å)	Polymer density (g/cm^3)	Φ	Wt. methanol (%)	N_{MeOH}	Wt. DMF (%)	N_{DMF}
40	0.97	0.60	3.7	45	6.2	34
45	0.68	0.42	26.5	421	31.9	241
50	0.50	0.31	43.9	917	47.8	470
55	0.37	0.23	56.1	1495	61.4	817
60	0.29	0.18	64.5	2130	⋯	⋯

Bulk liquid MD simulations of the different components that are considered in this study were performed using the Lekner summation method.[25] Columns 2 and 4 of Table IV contain values (in debye units) of the simulated mean molecular electric dipole moment μ^{liq} and simulated total fluid electric dipole moment $|\mathbf{M}|$. Column 3 contains gas phase electric dipole moment μ^{gas}.

For methylamine-methanol (mamine-MeOH) mixtures in Fig. 3(a), two primary solvation shells involving hydrogen atoms in the solvent and the reagent occur at about 2 Å. This indicates how the relatively small hydrogen atom permits close contact to more bulky oxygen or nitrogen atoms. Such bulky atoms are displaced at larger distances from each other, as can be seen in the peak at about 3 Å. This pattern continues with the methyl-methyl RDFs, with a peak occurring at about 4 Å. In addition, a second solvation shell can be seen in both of the RDFs involving hydrogen atoms. For methylamine-DMF mixtures in Fig. 3(b), a primary solvation shell involving hydrogen atoms in the reagent and oxygen in the solvent occurs at about 2 Å, with a second peak occurring at 3.5 Å. There is therefore some localized hydrogen bonding between methylamine and DMF but only at short distances. The solvent hydrogen is not involved in significant hydrogen bonding with the amino group of the reagent, despite the preferential ordering in this direction between the oxygen in DMF and hydrogens in methylamine. The solvent to reagent methyl group and c.m. RDFs contain primary solvation layers at 4 and 5 Å, respectively.

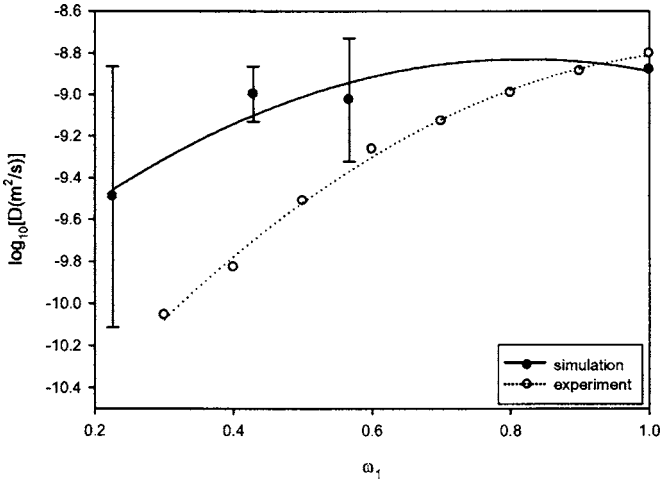

FIG. 6. Comparison of the simulated zero-field self-diffusion coefficient of DMF in *a*-PS solutions with experimental values determined using pulsed-gradient spin-echo NMR spectrometry over a range of solvent weight fractions at 25 °C.

Liquid dynamics

Evidence of strong Arrhenius diffusive behavior, conforming to a Wilke-Chang empirical fit[40] is shown in Fig. 4 for bulk liquid methanol and DMF over a range of temperatures. For liquid methanol, the Wilke-Chang empirical fit is coincident with the experimental value only when the association factor is set at unity ($\phi_e=1$). MTS^2 and MTS^3 denote two and three tiered multiple time step schemes[41] and these results were obtained using the Lekner summation method[25] to account for long-range electrostatic interactions in the bulk liquid over the course of 600 ps simulations. Internal molecular motion in the MTS^2 scheme allows bond angle bending but constrains bond lengths with the RATTLE algorithm,[42] whereas the MTS^3 scheme has the additional feature of bond length flexibility. It can clearly be seen that the MTS^2 scheme performs far better than the MTS^3 scheme for liquid methanol. It was therefore not possible to include bond length flexibility without disturbing the diffusive characteristics that accurately represent experimental values of self-diffusion coefficients. However, the MTS^3 scheme works best for liquid DMF, but not significantly better than the MTS^2 scheme because of additional inversion and torsion potentials which restrict the intramolecular motion in DMF to a planar conformation. For consistency, it was therefore reasonable to employ the MTS^2 scheme for each solvent in all further simulations, including those with an externally applied e/m field.

TABLE VII. Overview analysis of generic model of penetrant diffusion in polymers. PIB=polyisobutylene; PP=polypropylene; PDMS=poly(dimethylsiloxane); PE=polyethylene; HALS$_N$=hindered amine light stabilizer with N carbon atoms.

System: polymer/penetrant	D_{lit} (m^2/s$\times 10^{-9}$)	D_{model} (m^2/s$\times 10^{-9}$)
PIB/He[a]	1.00	1.44
PP/CO_2[b]	0.12	0.26
PP/He[b]	6.80	8.34
PP/CH_4[c]	0.05	0.02
PDMS/water[d]	1.53	0.71
PDMS/ethanol[d]	0.20	0.03
PE/water[e]	0.78	0.59
PE/ethanol[e]	0.07	0.09
PE/$HALS_3$[f]	0.87	0.66
PE/$HALS_{15}$[f]	0.43	0.49

[a]Reference 29.
[b]Reference 34.
[c]Reference 33.
[d]Reference 31.
[e]Reference 32.
[f]Reference 43.

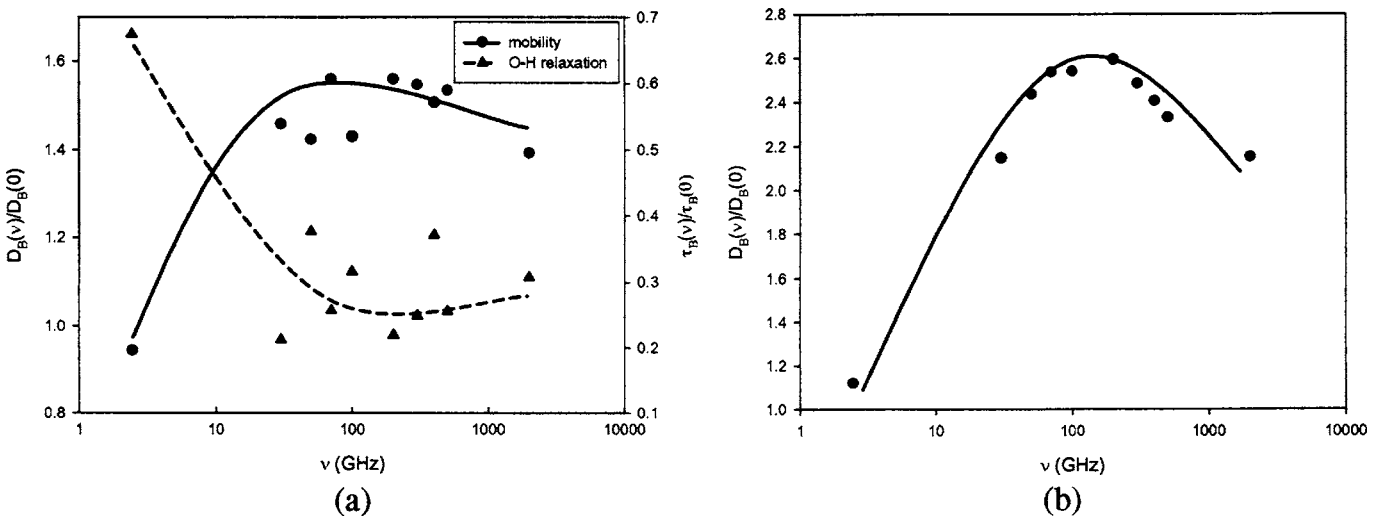

FIG. 7. Comparison of bulk solvent dynamics between field applied (rms electric field strength=0.1 V/Å) and field absent conditions over a range of frequencies at 25 °C obtained from MD simulations. (a) methanol mobility and O–H bond orientational relaxation times and (b) DMF mobility.

Table V contains values of the preexponential factors and activation energies determined using the simple Arrhenius relationship: $D=D_0e^{-E_D/k_BT}$, where k_B is Boltzmann's constant.

Using Eq. (27), a mutual diffusion coefficient for methylamine in methanol of 2.0×10^{-9} m^2/s was determined, compared to a Wilke-Chang value of 2.3×10^{-9} m^2/s. For methylamine in DMF, a mutual diffusion coefficient of 0.6×10^{-9} m^2/s was determined, compared to a Wilke-Chang value of 0.34×10^{-9} m^2/s.

Polymer structure

Figure 5 was obtained from a 100 ps simulation of dry atactic polystyrene at 25 °C and is consistent with the results of Mondello *et al.*[18] In addition to the main amorphous "halo" at a value of the scattering vector $q=1.3$ Å^{-1} in Fig. 5(b), a characteristic "polymerization peak" in the diffraction pattern at $q=0.75$ Å^{-1} can be observed. This feature arises from an *intermolecular* interference effect which has been reproduced using simulations of multiple chains of polystyrene.

Equilibration of polymer solutions

Table VI shows numerical values of the chemically equilibrated weight percentage of solvent and solvent particle number N for methanol-polystyrene and DMF-polystyrene solutions, averaged over three independent configurations at each polymer density. The simulation cell length L varies from 40 to 60 Å, although no value was determined for DMF at the lowest density.

Validation of zero field simulations of SPOS mixtures

Pulsed-gradient spin-echo NMR spectroscopy experiments were performed on DMF/*a*-PS solutions. Figure 6 compares the simulated and NMR experimental diffusion coefficients of DMF in *a*-PS at 298 K over a range of solvent weight fractions ω_1. It can be seen that there is a good agreement between the simulated and experimental results. The error bars report the 95% confidence intervals based on the three independent configurations.

The discrepancy between simulation and experiment is particularly noticeable at low solvent weight fractions where polymer-solvent interactions are reduced. This apparent enhanced solvent diffusion over experimental measurements can be attributed to three main factors associated with the simulated results: (i) a weak force field (shifted force LJ potential and no electrostatics on polymer) underestimates the strength of the interactions between solvent and polymer, (ii) use of finite molecular weight chains, and (iii) united atom groups on polymer. These zero-field results support the combined use of the chosen DMF and *a*-PS potential models and provide a basis for the forthcoming results with an externally applied e/m field. Due to technical limitations with the pulsed-gradient spin-echo method, it was not possible to obtain diffusion coefficients of methanol in polystyrene using NMR spectrometry.

Validation of generic model of self-diffusion

The results of an overview analysis of several reported results from the literature are presented in Table VII, in order to ascertain the validity of the generic model of diffusion that was proposed in Eq. (28). Table VII contains a list of simulated penetrant self-diffusion coefficients D_{lit} in various different penetrant/polymer systems that have been produced from the referenced computer simulations.

The last column in Table VII contains the penetrant self-diffusion coefficient D_{model} as determined with Eq. (28) and the mean-squared displacement data that were presented in the referenced material. By comparing the last two columns, one can make a reasonable assumption that the model works well and should therefore apply with polystyrene solutions. It can be noted, however, that for water and ethanol in poly(dimethylsiloxane) (PDMS), the linear fits that provide the literature values were not as accurate in comparison with the other values of diffusion coefficients by these authors.

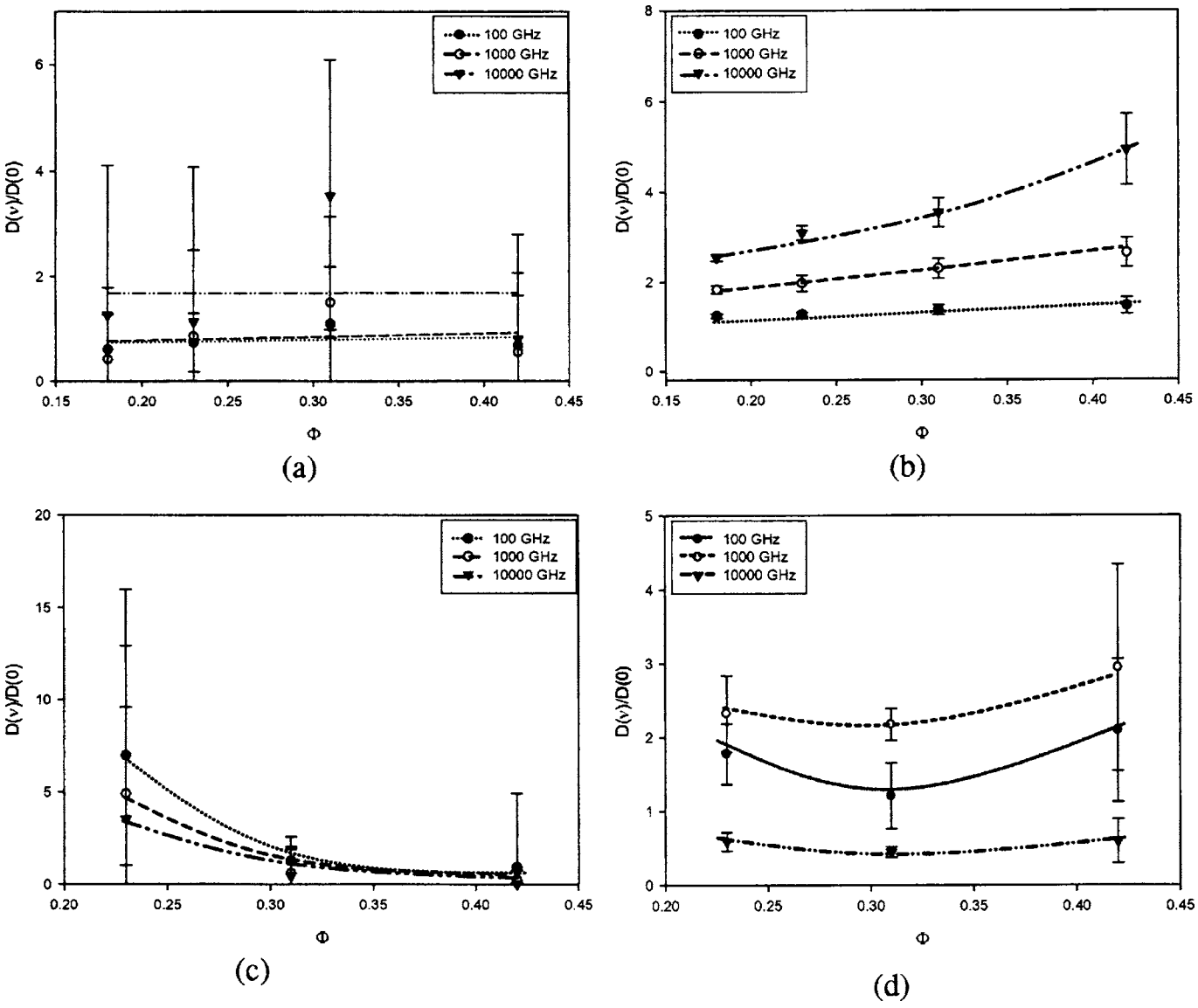

FIG. 8. Translational mobility in methylamine/solvent/*a*-PS solutions at 25 °C relative to zero field and conditions: (a) methylamine in methanol mixtures, (b) methanol, (c) methylamine in DMF mixtures, and (d) DMF.

Solvent dynamics in external electromagnetic field

Preliminary simulation studies on the molecular mobility of bulk liquid methanol and DMF in an external microwave field with a rms electric field intensity of 0.1 V/Å were performed in the *NVT* ensemble at 298 K using the MTS[2] scheme. This threshold value of the rms electric field strength was found to apply for bulk liquid methanol in a study of the effect of RMS electric field strength on translational and rotational molecular motion.[27] The enhancement in molecular mobility $D_B(\nu)$ relative to the zero field conditions $D_B(0)$ as the field frequency is increased is shown in Fig. 7(a), with a peak occurring just below 100 GHz. In addition, using Eq. (18), the reduction in the O–H bond relaxation time $\tau_B(\nu)$ relative to the zero field case $\tau_B(0)$ is also shown on the secondary ordinate axis. The zero field values of $D_B(0)$ and $\tau_B(0)$ were determined at 298 K to be 2.2×10^{-9} m^2/s and 1.86 ps, respectively.

The curves drawn represent the average behavior of the solvent over a range of e/m field frequencies. It is clear that as the mobility increases or decreases, the O–H bond orientational relaxation time behaves in the opposite sense. Hydrogen bonds are colinear with O–H bonds in methanol and any disruption of the hydrogen bond network allows for an increase in molecular mobility. A reduction in the orientational relaxation time of the O–H bond can be linked to a reduction in hydrogen bond lifetimes and less hindrance to molecular mobility.

Figure 7(b) illustrates the enhancement in translational mobility of bulk liquid DMF in an external e/m field. The simulated zero-field self-diffusion coefficient was determined to be 1.32×10^{-9} m^2/s, which closely agrees with the value determined by NMR at $\omega_1 = 1$, as shown in Fig. 6. DMF mobility is optimally excited at 100 GHz and by comparison with Fig. 7(a), the mobility enhancement in bulk liquid DMF is greater than with bulk liquid methanol.

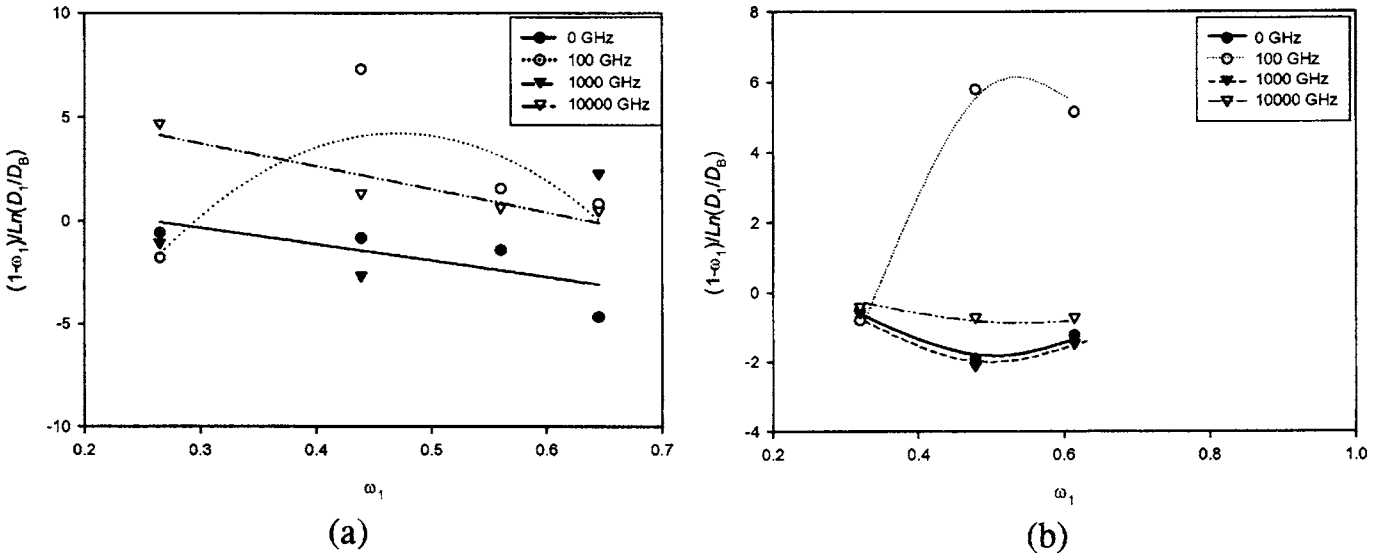

FIG. 9. Validation of the Vrentas-Duda model of solvent self-diffusion in polystyrene at 298 K over a range of electromagnetic field frequencies: (a) methanol and (b) DMF.

Translational molecular motion of SPOS mixtures in external electromagnetic field

The diffusion coefficients or mobilities of methanol and methylamine were determined using Eq. (28), with $n=0.5$, after establishing the behavior of $d(\log\langle\Delta r^2\rangle)/d\log(t)$ over the course of the sampling period of 100 ps, and applying the generic correlation to data outside the early time ballistic regime. The dependence of solvent and reagent transport on microwave field frequency and polymer density is depicted in Fig. 8. These figures are based on an averaging of diffusion results from three selected polystyrene configurations at each density shown in Table VI. The error bars at each density represent the error bounds on the averaged results at the 95% confidence level from samples of three independent configurations. The curves show general trends that indicate how the e/m field affects the solvent or reagent relative to the same polymer solutions under zero field conditions. Since Fickian diffusion was not approached for the solvent in the highest density systems, which approximate the dry polymer density, no mobility results have been included for these systems in Fig. 8.

In Figs. 8(a) and 8(b), it is apparent that the external microwave field induces the greatest enhancement of methylamine mobility and methanol mobility at intermediate polymer densities. Interestingly, it was found that the cross-correlation between methanol dipole rotation and methylamine translational velocity is greatest at $\Phi=0.3$.[27] One can therefore appreciate that induced methanol dipole oscillations, caused by the external e/m field, have a significant effect on methylamine transport, particularly in a polystyrene environment of this density. The mobility enhancement relative to diffusion in the polymer under zero field conditions occurs at higher densities for solvent methanol. Methanol mobility within the polymer appears to increase

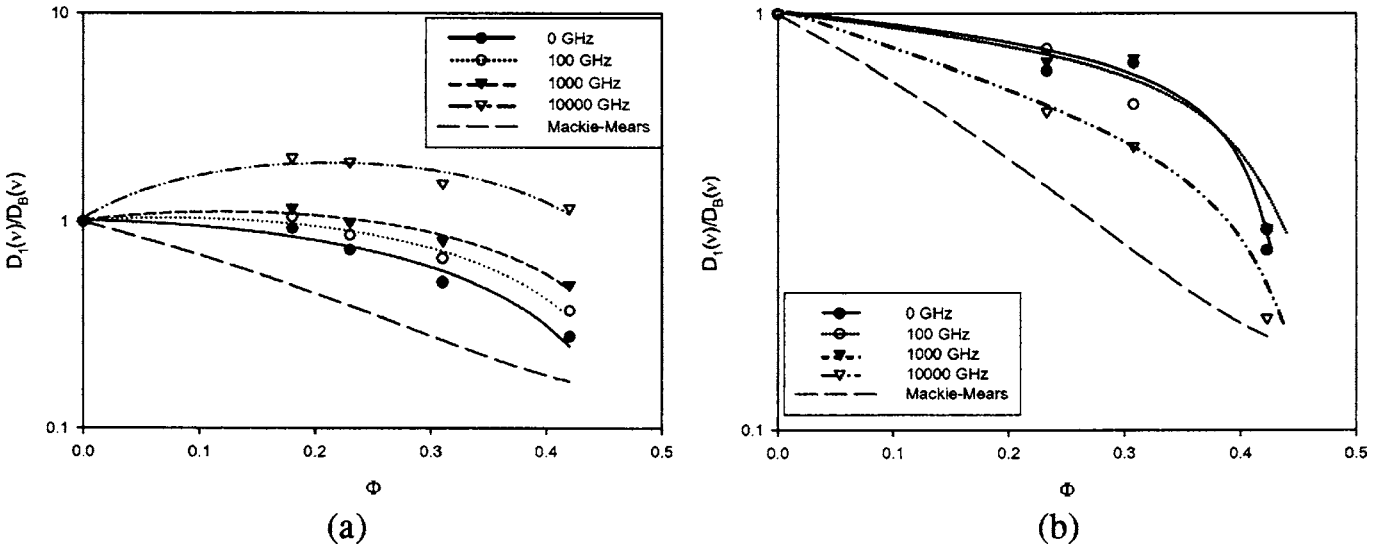

FIG. 10. Solvent self-diffusion coefficient in atactic polystyrene relative to the bulk liquid over a range of polymer densities under identical field conditions at 298 K: (a) methanol and (b) DMF.

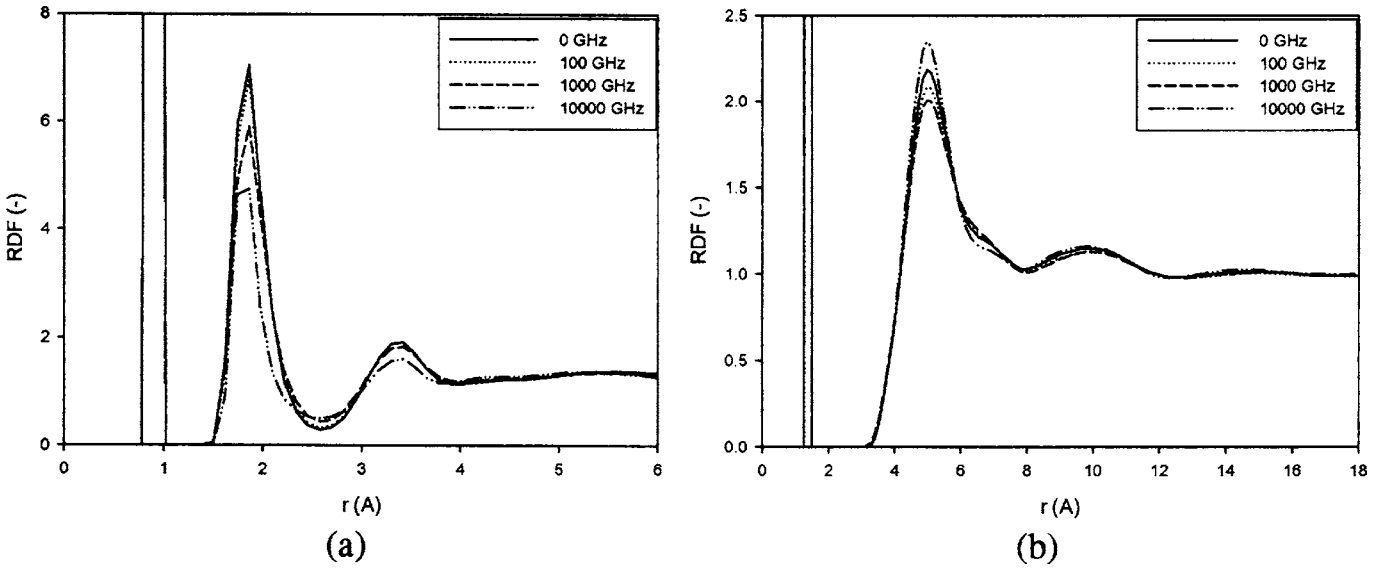

FIG. 11. Heteroatomic RDFs at 25 °C in methylamine/solvent/*a*-PS solutions (*a*-PS density=0.5 g/cm^3) over a range of frequencies and a rms electric field intensity of 0.1 V/Å: (a) methanol O–H and (b) DMF C–O.

steadily with frequency, with the increase being the more remarkable at the highest polymer density within which Fickian diffusion was approached. It is anticipated that chains of hydrogen bonded methanol molecules bound within *a*-PS are significantly smaller in length than the average chain length of 15.5 methanol molecules in the bulk liquid[44] on account of a physical disruption caused by the presence of the polymer backbones and pendant groups. The mobilities of methanol in *a*-PS and the associated methylamine reagent are greatest at 10^4 GHz.

Furthermore, with regard to the dependence of reagent transport on frequency, methylamine mobility increases sharply at 100 GHz, steadily at 1000 GHz, and sharply again at 10^4 GHz. Methanol dipolar rotation is significantly arrested at 100 GHz due to resonance with the molecular dipole moment. Likewise, at 10^4 GHz, methanol rotations are hindered by the extremely high frequency of the alternating field. Molecular rotation shall be considered in more detail in future studies of polystyrene solutions in microwave fields. Under such conditions, it can be imagined that relatively long-lived tunnels are formed by methanol molecules through which methylamine can move.

Figures 8(c) and 8(d) for methylamine/DMF/*a*-PS solutions are analogous to Figs. 8(a) and 8(b) for methylamine/methanol/*a*-PS solutions. The most significant enhancement in methylamine mobility appears to take place at low polymer densities and maximized at 100 GHz. In Fig. 8(d), the frequency ordering of the curves is different to methanol and DMF mobility enhancement is greatest at 1000 GHz. Methylamine mobility is more significantly enhanced in DMF/*a*-PS solutions than in methanol/*a*-PS solutions. However, DMF mobility enhancement is lower than the corresponding values

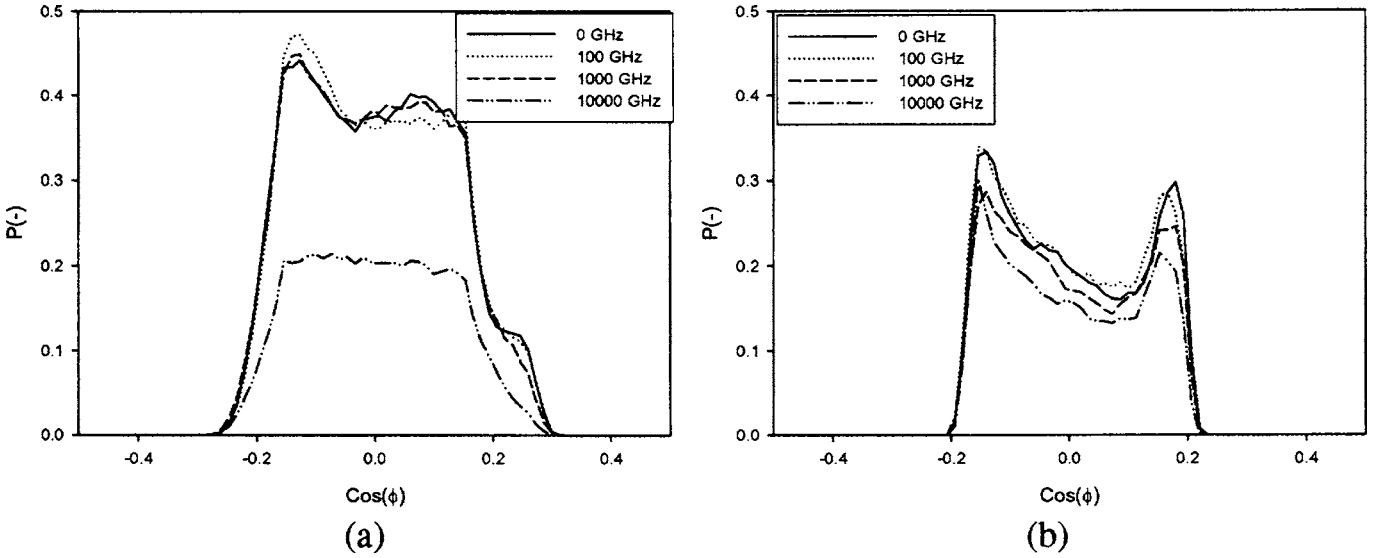

FIG. 12. Orientation of solvent in a 6.5 Å cosphere of a single methylamine reagent at 25 °C in methylamine/solvent/*a*-PS solutions (*a*-PS density =0.5 g/cm^3) over a range of frequencies and a rms electric field intensity of 0.1 V/Å: (a) solvent methanol/*a*-PS solutions and (b) methylamine/DMF/*a*-PS solutions.

TABLE VIII. Methanol and DMF residence times at 298.0 K in solvent cosphere of methylamine (cosphere radius=6.5 Å, *a*-PS density =0.5 g/cm^3, and E_{rms}=0.1 V/Å).

ν (GHz)	$\langle\tau_{RT}\rangle_{MeOH}$ (ps)	$\langle\tau_{RT}\rangle_{DMF}$ (ps)
0	2.68	2.88
100	2.53	2.73
1000	2.30	2.49
10000	1.98	2.77

in methanol/*a*-PS solutions. This is in contrast to the bulk solvent behavior shown in Fig. 7. Further studies on the dynamics of these solutions over a range of e/m field frequencies at a fixed intermediate polymer density are investigated in the next section.

Equations (29) and (30) were used as a test of a phenomenological description of solvent diffusion in polymers under both zero field conditions and in an electromagnetic field environment. The data for methanol and DMF diffusion in *a*-PS can be seen in Figs. 9 and 10, which compare the Vrentas-Duda model and the Mackie-Mears model, respectively. It can be seen that the Vrentas-Duda model of methanol self-diffusion is approached only under conditions of zero field or very high field frequencies. At intermediate field frequencies, this model is not appropriate as an approximation. At 1000 GHz, in particular, the solvent self-diffusion coefficient in *a*-PS approaches the value in the bulk liquid $[D_1(1000)/D_B(1000)=0.996]$ and a sharp negative deviation occurs with an ordinate value of −104.6, not shown in Fig. 9. This corresponds to the second point in Fig. 10(a) for the 1000 GHz curve. In Fig. 9(b), the self-diffusion of DMF in *a*-PS conforms to the Vrentas-Duda model of penetrant diffusion under experimental zero-field conditions and simulated field applied conditions at 10^4 GHz, only. As with methanol/*a*-PS systems, the model is clearly not adhered to at intermediate frequencies.

In Fig. 10(a), the methanol self-diffusion diffusion coefficients in *a*-PS are normalized by the corresponding values in the bulk liquid phase (to which quasiequilibrium has been established) under identical field conditions. The parameter-free Mackie-Mears model represents the motion of a nonpolar solvent in *a*-PS under all field conditions. By introducing polarity into the solvent component of the system, a clear separation from simple geometrically hindered motion occurs, which increases in extent with increasing field frequency. A maximum can also be observed with each curve over 100 GHz and this occurs at the lowest polymer volume fraction. Such maxima highlight the enhanced mobility of methanol within the polymer relative to the mobility in the bulk liquid under identical field conditions. It is therefore apparent that the presence of the polymer increases the *absolute* methanol mobility under nonzero field conditions in the gigahertz region. In Fig. 10(b), the ordinate remains below unity in all cases and therefore diffusion of DMF is hindered by the presence of the polymer.

Effect of electromagnetic field frequency on structural and dynamical behavior of SPOS mixtures

The following series of figures examines the effect of e/m field frequency on various structural and dynamical results in methanol/*a*-PS and DMF/*a*-PS solutions. A polymer density of 0.5 g/cm^3 was used in these investigations and the results have been averaged over three configurations.

In order to understand some of the dynamic features that are present in methanol/*a*-PS solutions over a range of e/m frequencies, the effect of e/m frequency on the extent of hydrogen bonding in methanol can be seen in Fig. 11(a). A reduction in the oxygen-hydroxyl hydrogen first peaks with increasing e/m field frequency can be noted. The reduction in methanol structure can be rationalized by the breakup of hydrogen bonding which occurs to the greatest extent at 10^4 GHz. The intermolecular carbon-oxygen structure in DMF bound within *a*-PS decreases with increasing frequency up to 1000 GHz, as shown in Fig. 11(b), but then

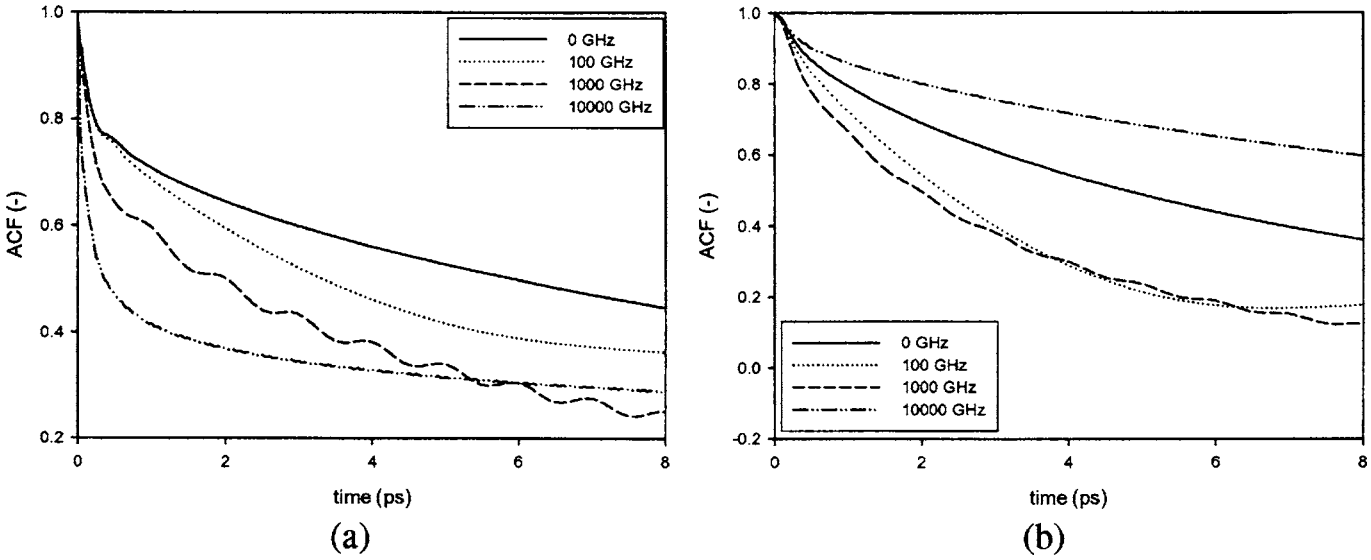

FIG. 13. Solvent molecular dipole ACF at 25 °C in methylamine/DMF/*a*-PS solutions (*a*-PS density=0.5 g/cm^3) over a range of frequencies and a rms electric field intensity of 0.1 V/Å. (a) Methanol and (b) DMF.

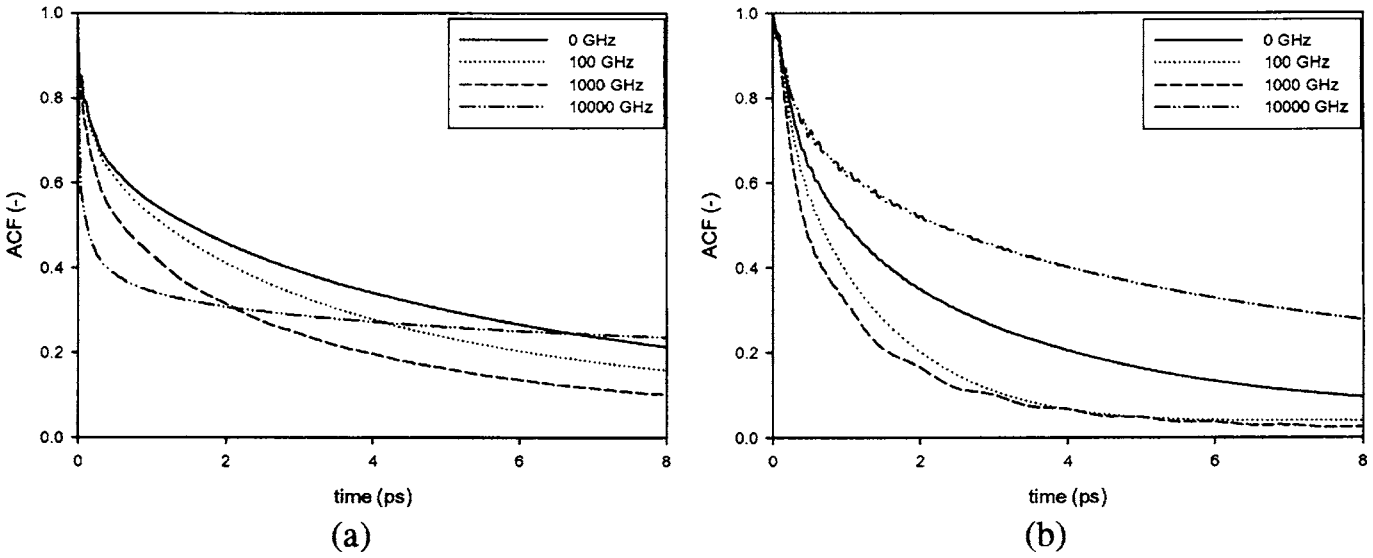

FIG. 14. $C_2(t)$ bond rotational ACFs at 25 °C in methylamine/solvent/*a*-PS solutions (*a*-PS density=0.5 g/cm^3) over a range of frequencies and a rms electric field intensity of 0.1 V/Å: (a) methanol O–H and (b) DMF C–O.

increases above the zero field level at 10^4 GHz. This behavior applies for all three solvation layers, which can be discerned in Fig. 11(b). The corresponding intramolecular peak does not vary with frequency up to 10^4 GHz.

The effect of e/m field frequency on the orientation of methanol in a 6.5 Å cosphere of the reagent can be seen in Fig. 12(a), where a considerable drop in the peak height of the distribution occurs between 1000 and 10^4 GHz. In addition, the shape of the curve at 10^4 GHz displays a single broad peak as opposed to a bimodal distribution at lower frequencies. It can be concluded that the solvation shell has become depopulated and can be attributed to a reduction in hydrogen bonding structure, as shown in Fig. 11. The range of angles spanned by these distributions is approximately 80° up to about 100°. Referring to Fig. 1, one can picture a sphere of methanol dipoles, about the methylamine reagent, randomly pointing slightly inwards or outwards to a fairly even extent at 10^4 GHz. At 100 GHz, in particular, however, the dipole moment vector becomes more directed away from the reagent. The orientations of methanol dipoles about methylamine therefore appear to exhibit considerable structural features up to at least 1000 GHz, but which ceases to exist by at most 10^4 GHz. In Fig. 12(b), the orientation of DMF in a 6.5 Å cosphere of methylamine can be seen to be highly structured up to 10^4 GHz. A bimodal distribution indicates two antiparallel conformations of DMF about the reagent. This feature occurs to a lesser extent with methanol up to 1000 GHz in Fig. 12(a).

Table VIII contains the mean residence times of solvent within a 6.5 Å cosphere of the reagent in *a*-PS solutions with a polymer density of 0.5 g/cm^3, as determined using Eq. (21).

The molecular dipole moment autocorrelation functions (ACFs) for methanol and DMF over a range of e/m field

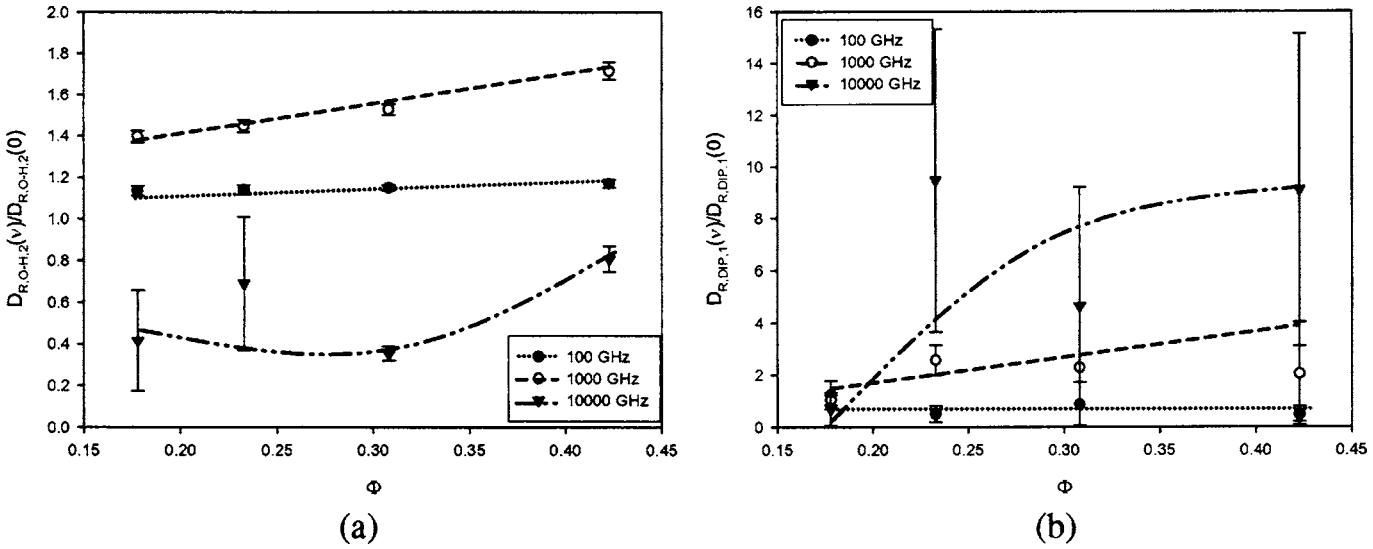

FIG. 15. Rotational diffusion coefficient at 25 °C in methylamine/methanol/*a*-PS solutions over a range of frequencies and polymer densities and at a rms electric field intensity of 0.1 V/Å: (a) methanol O–H and (b) methylamine molecular dipole.

TABLE IX. O–H bond rotational diffusion coefficient $D_{R,O-H,2}(v)$ (ps^{-1}) in methylamine/methanol/*a*-PS solutions at 25 °C.

L (Å)	A	B	C	Average
45	0.049	0.051	0.051	0.051
50	0.055	0.056	0.056	0.056
55	0.061	0.059	0.060	0.060
60	0.065	0.065	0.063	0.064

frequencies at 25 °C and a polymer density of 0.5 g/cm^3 are shown in Fig. 13. The periodicity of the e/m field is apparent only at 1000 GHz over the sampling period of 8 ps, at which frequency there is also a rapid decay of the ACFs for both methanol and DMF. A slow decay of the ACF for DMF (below the zero-field level) occurs at 10^4 GHz, in contrast to the behavior of methanol, which shows a long-lived decay after 8 ps.

The variation of the O–H bond $C_2(t)$ ACF for methanol over the same range of conditions is displayed in Fig. 14(a) and illustrates a rapid decay at 1000 GHz and a very slow decay at 10^4 GHz below the zero field level at 10^4 GHz. In contrast, no delay was found with the N–H bond $C_2(t)$ ACF for methylamine in methanol/*a*-PS solutions.[27] The variation of the C–O bond $C_2(t)$ ACF for DMF is displayed in Fig. 14(b), where the same frequency pattern appears as with the molecular dipole moment ACF for DMF.

Rotational molecular motion of SPOS mixtures in external electromagnetic field

Both the molecular dipole ACFs and molecular bond rotational ACFs can be used to obtain rotational diffusion coefficients using Eq. (20). Figure 15(a) illustrates how rotational motion of the O–H bond in methanol is enhanced above the zero field values at 100 and 1000 GHz over the full range of polymer densities. As before, these results are averaged over three independent configurations at each polymer density. The enhancement is not large at 100 GHz and largely independent of polymer density. At 10^4 GHz the O–H rotational motion is considerably reduced relative to zero field conditions, with a slight decrease occurring at about $\Phi=0.3$ and 10^4 GHz. This is precisely the value when methylamine enhancement is a maximum, as shown in Fig. 8(a). The numerical values of the zero-field absolute O–H bond rotational diffusion coefficients of methanol are shown in Table IX. There is clearly a greater level of rotation at lower polymer densities. In contrast to the behavior of methanol, the enhancement of the methylamine molecular dipole rotational diffusion coefficient in methanol/*a*-PS solutions appears greatest at 10^4 GHz in Fig. 15(b), supporting the notion of a tunneling mechanism of translational reagent diffusion.

Figure 16 illustrates the dependence of the molecular dipole orientation rotational diffusion coefficient of methanol and DMF over a range of polymer densities and e/m field frequency. The zero-field values are listed in Tables X and XI. It is apparent from Fig. 16(a) that at low to intermediate polymer densities, the frequency ordering of the enhancement in methanol molecular dipole orientation rotational diffusion coefficient is opposite that of the enhancement in methanol translational diffusion coefficient, illustrated earlier in Fig. 8(b). It can also be noted that the curves for 100 and 10^4 GHz are below the zero-field level, except at high polymer densities where significant hindrance to molecular rotation exists with and without the e/m field. Likewise in Fig. 16(b), there is significant retardation of molecular dipole rotation of DMF below the zero-field level at 10^4 GHz. At this frequency in Fig. 8(d), the translational mobility of DMF was also found to be significantly reduced. This is expected for the planar DMF molecule. DMF is required to rotate in order to translate through polystyrene, particularly since it can become lodged close to the polymer backbone, as shown by RDF analysis.[27] In contrast, molecules of methanol tend to permeate the polymer network with or without molecular rotations and can therefore better utilize the interconversion of rotational and translation kinetic energy.

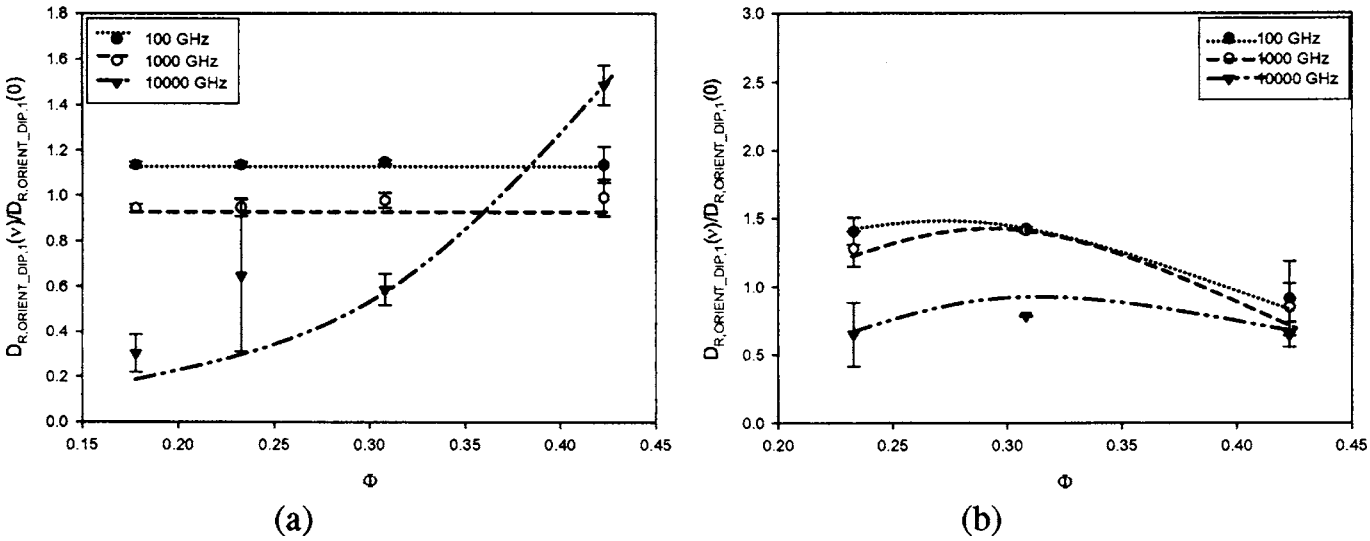

FIG. 16. Solvent molecular dipole orientation rotational diffusion coefficient relative to zero field conditions at 25 °C in methylamine/solvent/*a*-PS solutions over a range of frequencies and polymer densities and at a rms electric field intensity of 0.1 V/Å: (a) methanol and (b) DMF.

TABLE X. Methanol molecular dipole orientation rotational diffusion coefficient $D_{R,\mathrm{dip},1}(v)$ (ps^{-1}) in methylamine/methanol/*a*-PS solutions at 25 °C.

L (Å)	A	B	C	Average
45	0.103	0.120	0.098	0.107
50	0.108	0.109	0.109	0.109
55	0.113	0.112	0.112	0.113
60	0.117	0.117	0.114	0.116

CONCLUSIONS

The dynamics of methanol, DMF, and methylamine in chemically balanced polystyrene solutions under an externally applied e/m field and over a range of polymer densities was examined using MD simulations in the *NVT* ensemble. The zero field self-diffusion coefficients of DMF in *a*-PS were found to closely agree with experimental NMR values, although discrepancies can be attributed to weaker potential interactions in the simulations in comparison to reality. Bulk liquid self-diffusion coefficients conformed to a Wilke-Chang empirical correlation on an Arrhenius plot. These results provided a sound basis for the combined use of the chosen solvent and polymer potential models and allowed the simulated results with an external e/m field to be treated with confidence. Although modern industrial and experimental microwave apparatus employ e/m field strengths which are several orders of magnitude lower than those studied here, it was necessary to use rms electric field strengths of 0.1 V/Å due to the current sampling times that are accessible in computer simulations of systems involving up to about 10 000 atoms.

It has been determined that molecular mobility can be significantly enhanced by applying an external electromagnetic radiation field. The degree of enhancement can be tailored for different types of molecular systems by adjusting the frequency and strength of the applied e/m field. At a frequency of 100 and 10^4 GHz and a rms electric field strength of 0.1 V/Å, methylamine mobility in polystyrene/methanol solutions sharply increases. A molecular mechanism for this anomaly has been established with the dipole relaxation rate of methanol, which undergoes a comparably sharp retardation at 100 and 10^4 GHz. At these frequencies, methylamine rotation is significantly mobilized and methanol rotation is relatively immoblized. Since methanol is of comparable size to methylamine, this allows methylamine transport to take place with relatively little hindrance. Under such conditions, a methylamine molecule is more likely to circumvent a moderate potential barrier than a methanol molecule due to a bias in rotational molecular motion caused by the external e/m field. It is clear therefore that this is an athermal phenomenon that relates to the coupling of molecular dipoles to the e/m field in such a manner as to expose tunnels through which reagent transport can be facilitated.

TABLE XI. DMF molecular dipole orientation rotational diffusion coefficient $D_{R,\mathrm{dip},1}(v)$ (ps^{-1}) in methylamine/methanol/*a*-PS solutions at 25 °C.

L(Å)	A	B	C	Average
45	0.104	0.157	0.136	0.133
50	0.110	0.109	0.108	0.109
55	0.095	0.106	0.104	0.102

The planar DMF molecule can access the interstices of the polymer with suitable reorientation. DMF molecular dipole reorientation can be induced by an external application of an e/m field up to 1000 GHz. This provides excellent opportunity to enhance DMF mobility in *a*-PS using an e/m field. The large size and polar nature of the DMF molecule attributes it with good swelling properties and activity in the e/m field. DMF has already been successful in the coupling of peptides in the presence of e/m fields.[45] It is therefore effective in the presence of amine groups. The chemical identity of a solvent used to house the reagent and swell the polymer has particular importance to the economics of the drug formation process. Future studies shall therefore incorporate dichloromethane as a solvent in *a*-PS solutions with methylamine reagent in order to extend the scope of this research to relate to a wider area of reactions that are regularly processed in SPOS. Microwave heating of these polymer solutions shall also be examined using NEMD.

ACKNOWLEDGMENTS

One of the authors (M.P.) wishes to acknowledge a Ph.D. research scholarship (SC/2001/242) from Enterprise Ireland and many useful discussions with Thomas McDermott and Dr. Niall English.

[1] M. T. Ende and N. S. Peppas, J. Controlled Release **48**, 47 (1997).
[2] P. Gupta, K. Vermani, and S. Garg, Drug Discovery Today **7**, 569 (2002).
[3] Y. Qiu and K. Park, Adv. Drug Delivery Rev. **53**, 321 (2001).
[4] C. Neipp, A. Belendez, J. T. Sheridan, J. V. Kelly, F. T. O'Neill, S. Gallego, M. Ortuno, and I. Pascual, Opt. Express **11**, 1835 (2003).
[5] J. T. Sheridan, M. G. Gleeson, J. V. Kelly, and F. T. O'Neill, Opt. Lett. **30**, 239 (2005).
[6] B. M. Trost, K. Hiroi, and S. Kurozumi, J. Am. Chem. Soc. **97**, 440 (1975).
[7] H. Yu, S. T. Chen, and K. T. Wang, J. Org. Chem. **57**, 4781 (1992).
[8] M. Larhead, G. Lindeberg, and A. Hallberg, Tetrahedron Lett. **37**, 8219 (1996).
[9] M. Andreas, L. Hoel, and J. Nielsen, Tetrahedron Lett. **40**, 3941 (1999).
[10] G. J. Kuster and H. W. Scheeren, Tetrahedron Lett. **41**, 515 (2000).
[11] Y. Nakai, Y. Tsujita, and H. Yoshimizu, Desalination **145**, 375 (2002).
[12] W. L. Jorgensen, J. Phys. Chem. **90**, 1276 (1986).
[13] M. Chalaris and J. Samios, J. Chem. Phys. **112**, 8581 (1998).
[14] R. W. Impey, M. Sprik, and M. L. Klein, J. Am. Chem. Soc. **109**, 5900 (1987).
[15] S. L. Mayo, B. D. Olafson, and W. A. Goddard, J. Phys. Chem. **94**, 8897 (1990).
[16] H. Ohtaki, S. Itoh, T. Yamaguchi, S. Ishiguro, and B. M. Rode, Bull. Chem. Soc. Jpn. **56**, 3406 (1983).
[17] G. Schultz and I. Hatzittai, J. Phys. Chem. **97**, 4966 (1993).
[18] M. Mondello, H. J. Yang, H. Furuya, and R. J. Roe, Macromolecules **27**, 3566 (1994).
[19] G. Ciccotti and J. P. Ryckaert, Comput. Phys. Rep. **4**, 345 (1986).
[20] M. Müller, Ph.D. thesis, Swiss Federal Institute of Technology, 1999.
[21] D. Yoon, P. R. Sundararajan, and P. J. Flory, Macromolecules **6**, 776 (1975).
[22] P. Robyr, M. Müller, and U. W. Suter, Macromolecules **32**, 8681 (1999).
[23] N. J. English and J. M. D. MacElroy, J. Chem. Phys. **118**, 1589 (2003).
[24] M. P. Allen and D. J. Tildesley, *Computer Simulation of Liquids*, 1st ed. Oxford: Clarendon Press (1987).
[25] J. Lekner, Physica A **176**, 485 (1991).
[26] B. Knopp, U. W. Suter, and A. A. Gusev, Macromolecules **30**, 6107 (1997).
[27] M. J. Purdue, Ph.D. thesis, University College, Dublin, 2005.

[28] M. Kotelyanskii, N. J. Wagner, and M. E. Paulitis, Comput. Theor. Polym. Sci. **9**, 301 (1999).
[29] A. A. Gusev and U. W. Suter, J. Chem. Phys. **99**, 2228 (1993).
[30] A. A. Gusev, S. Arizzi, U. W. Suter, and D. J. Moll, J. Chem. Phys. **99**, 2221 (1993).
[31] Y. Tamai, H. Tanaka, and K. Nakanishi, Macromolecules **27**, 4498 (1994).
[32] Y. Tamai, H. Tanaka, and K. Nakanishi, Fluid Phase Equilib. **104**, 363 (1995).
[33] F. Müller-Plathe, J. Chem. Phys. **96**, 3200 (1992).
[34] T. R. Cuthbert, N. J. Wagner, M. E. Paulaitis, G. Murgia, and B. D'Aguanno, Macromolecules **32**, 5017 (1999).
[35] F. Müller-Plathe, S. C. Rogers, and W. F. van Gunsteren, Chem. Phys. Lett. **199**, 237 (1992).
[36] J. H. D. Boshof, R. F. Lobo, and N. J. Wagner, Macromolecules **34**, 6107 (2001).
[37] D. Marquardt, SIAM J. Appl. Math. **11**, 431 (1963).
[38] J. S. Vrentas and J. L. Duda, J. Polym. Sci., Polym. Phys. Ed. **15**, 403 (1977).
[39] F. Müller-Plathe, Chem. Phys. Lett. **252**, 419 (1996).
[40] R. H. Perry and D. W. Green, *Perry's Chemical Engineers Handbook*, 7th ed. (McGraw-Hill, New York, 1997).
[41] G. J. Martyna, M. E. Tuckerman, and M. L. Klein, J. Chem. Phys. **97**, 2635 (1992).
[42] H. C. Anderson, J. Comput. Phys. **52**, 24 (1983).
[43] S. K. Nath, J. J. de Pablo, and A. D. DeBellis, J. Am. Chem. Soc. **121**, 4252 (1999).
[44] M. Matsumoto and K. E. Gubbins, J. Chem. Phys. **93**, 1981 (1990).
[45] H. Yu, S. T. Chen, and K. T. Wang, J. Org. Chem. **57**, 4781 (1992).